Variations in Apparent Mixing Efficiency in the North Atlantic Central Water

BARRY RUDDICK AND DAVID WALSH

Department of Oceanography, Dalhousie University, Halifax, Nova Scotia, Canada

NEIL OAKEY

Physical and Chemical Sciences, Department of Fisheries and Oceanography, BIO, Dartmouth, Nova Scotia, Canada

(Manuscript received 7 April 1997, in final form 14 May 1997)

ABSTRACT

Microstructure data from the North Atlantic Tracer Release Experiment (NATRE) are presented, providing detailed profiles of the thermal variance χ in the upper 360 m of the Canary Basin for the fall and spring seasons. The Osborn–Cox model is used to compute the diffusivity K_T. The diffusivity for the depth range 240–340 m is found to be $1.0(\pm 0.04) \times 10^{-5}$ m^2 s^{-1} in the fall and $2.2(\pm 0.1) \times 10^{-5}$ m^2 s^{-1} in the spring, in good agreement with dye-inferred diffusivities at similar depths. Measured turbulent kinetic energy (TKE) dissipation rates were found to be contaminated by hydrodynamic noise, so the Osborn dissipation method was not used to compute K_ρ. However, data segments for which the TKE dissipation rate (ε) was large enough to be unaffected by noise were used to compute the ''apparent mixing efficiency'' Γ_d. The computed Γ_d values are used to investigate variations in apparent mixing efficiency with respect to density ratio (R_ρ) and turbulence Reynolds number [$\varepsilon/(\nu N^2)$], in an attempt to elucidate the underlying mechanisms of mixing in the NATRE region. Observed variations of Γ_d are compared with existing theoretical models of mixing due to: salt fingers, a combination of salt fingers and turbulence, ''conventional'' high Reynolds number turbulence, and low Reynolds number buoyancy-modified turbulence. Significant variations of Γ_d with respect to both R_ρ and $\varepsilon/(\nu N^2)$ are found. Although Monte Carlo tests show that some of the observed variations could be noise-induced, a substantial portion of the systematic variations the authors observed were not reproduced by Monte Carlo simulations. These trends are found to be statistically significant, and the authors conclude that they represent real variations in the apparent mixing efficiency. The authors find that Γ_d is an increasing function of $\varepsilon/(\nu N^2)$ and a decreasing function of R_ρ; these variations are not fully consistent with any of the available mixing models.

1. Introduction

The North Atlantic Tracer Release Experiment (NATRE) was one of the Core-3 process experiments performed as part of the World Ocean Circulation Experiment (Ledwell et al. 1993; Ledwell and Watson 1994). In April 1992, sulfur hexafluoride was released within a few meters of the $\sigma_t = 28.036$ isopycnal surface near 300-m depth. Its lateral dispersion and vertical spreading via diapycnal mixing processes were observed in subsequent surveys during the following year. The spreading rate was consistent with a diapycnal diffusivity of 1–2 ($\times 10^{-5}$ m^2 s^{-1}), with the larger value occurring in the winter months.

In order to explore the links between finestructure, microstructure, and diapycnal mixing, and to test the methods and models currently used to infer mixing rates from microstructure measurements, nearly two thousand profiles of the vertical gradients of microscale temperature and velocity were taken using the tethered profiler EPSONDE (Oakey 1988). The instrument was also equipped with conventional CTD sensors to relate the microstructure observations to water masses and to local vertical gradients of temperature, salinity, and density. The main rationale for verification of microstructure methodologies is cost: Tracer experiments require a great deal of ship-time due to sampling requirements, and microstructure measurements can be used to extrapolate the NATRE findings to other depths, times, and physical locations. The microstructure measurements and ancillary finescale observations also provide valuable clues as to the underlying physical mechanisms causing the mixing. It is important to understand the mechanisms so that suitable parameterizations can be devised for use in numerical circulation models, and to forecast the likely changes in mixing rate that might occur as a result of climate shifts.

In this paper, we explore the variation of a key observable, the apparent mixing efficiency, within the NATRE dataset in order to test the hypothesis that the observed microstructure is associated with ''conventional'' high Reynolds number turbulence. In the next section,

Corresponding author address: Dr. Barry Ruddick, Department of Oceanography, Dalhousie University, Halifax, NS B3H 4J1, Canada. E-mail: barry.ruddick@dal.ca

we summarize the classical models used to interpret microstructure observations, Gargett's (1988b) scaling arguments for buoyancy-modified turbulence, and models involving salt fingers. In section 3 we examine depth variation of diffusivity and compare with that inferred from the tracer. Our TKE dissipation measurements are found to have a noise problem, so that only the most intense data segments can be used for further analysis. In section 4 we examine the systematic variation of apparent mixing efficiency with environmental parameters, particularly gradient density ratio

$$R_\rho = \frac{\alpha T_z}{\beta S_z}, \tag{1}$$

(where the subscript z indicates partial differentiation) and turbulence activity parameter $\varepsilon/\nu N^2$. Finally, in section 5 we discuss the physical implications of our findings.

2. Models for interpretation of microstructure

Gregg (1987) reviews the traditional models used to interpret microstructure observations in terms of diapycnal diffusivities. We will summarize two of the models here in order to explain the computation and physical meaning of Γ_d. We also review microstructure models involving salt fingers to consider the possibility that double-diffusive fluxes play a role in this region.

a. The Osborn and Cox (1972) model

This model uses the concept that turbulent eddy transport of temperature $\overline{w'T'}$ down[1] a mean temperature gradient $\partial\overline{T}/\partial z$ will transport fluid parcels to regions where their temperature is anomalous, producing thermal variance $\overline{T'^2}$, which would increase indefinitely unless dissipated. The overbar indicates an average over scales slightly larger than turbulent length scales (in this case an average over the ~8 m data block length), and the prime indicates deviations from that average. Molecular diffusion of heat with diffusivity κ_T causes the anomalous blobs to blend into the background, and it is this diffusive blending that is estimated by microscale temperature sensors and is used in the Osborn–Cox model. After performing the Reynolds decomposition, the equation describing the budget of turbulent thermal variance is (Gregg 1987)

$$\underbrace{\frac{\partial\overline{T'^2}}{\partial t}}_{1} + \underbrace{\frac{\partial}{\partial x_i}\left[\overline{u}_i\overline{T'^2} + \overline{u_i'T'^2} - \kappa_T\overline{\left[\frac{\partial T'^2}{\partial x_i}\right]}\right]}_{2} + \underbrace{2\overline{u_i'T'}\frac{\partial\overline{T}}{\partial x_i}}_{3} = \underbrace{-2\kappa_T\overline{\left[\frac{\partial T'}{\partial x_i}\right]^2}}_{4}. \tag{2}$$

The first term represents the rate of change of thermal variance; term 2 is the divergence of the transport by the mean flow, the turbulence, and molecular diffusion, respectively. The third term represents production of thermal variance by lateral heat fluxes in a lateral temperature gradient ($i = 1, 2$) and by vertical heat flux in a vertical temperature gradient. The lateral terms may dominate in regions where lateral thermohaline intrusions occur (Gregg 1987). But since the lateral gradients are weak in the NATRE observations, we assume the vertical production term 3 (with $i = 3$) dominates on the left and is balanced by the dissipation term 4 on the right side of (2).

Under the above assumptions, and introducing the eddy diffusivity as the ratio of thermal eddy flux and temperature gradient, (2) reduces to (Osborn and Cox 1972)

$$K_T \equiv -\overline{w'T'}\Big/\overline{\left[\frac{\partial\overline{T}}{\partial z}\right]} = \chi/2\overline{\left[\frac{\partial\overline{T}}{\partial z}\right]^2}, \tag{3}$$

where

$$\chi = 2\kappa_T\overline{\left[\frac{\partial T'}{\partial x_i}\right]^2} \approx 6\kappa_T\overline{\left[\frac{\partial T}{\partial z}\right]^2}$$

(assuming isotropy) is the rate of dissipation of thermal variance by molecular diffusion. So long as a quasi-steady, homogeneous local balance obtains, with the vertical fluxes dominant, (3) is valid whether the vertical mixing is due to mechanically generated turbulence, salt fingers, or a combination of the two (Hamilton et al. 1993). The natural variability of χ (usually several orders of magnitude) and the skewness of its statistical distribution (Baker and Gibson 1987) requires that a large number of profiles be taken and averaged appropriately to obtain reliable diffusivity estimates. This has prevented the widespread use of the method.

b. The Osborn (1980) dissipation method

This method is based on the turbulent kinetic energy budget, and uses observations of the dissipation rate of turbulent kinetic energy (TKE) by molecular viscosity to infer the strength of the turbulent energy source, and hence infer the buoyancy flux. The TKE equation for stratified shear flow in the x_1 direction is (Gregg 1987)

[1] Downward turbulent heat flux implies transport of warm water parcels down to cooler (deeper) levels, where they are anomalously warm and appear as thermal fluctuations.

$$\frac{\partial}{\partial t}\overline{\left[\frac{\overline{\rho}\,u_j' u_j'}{2}\right]} + \frac{\partial}{\partial x_i}\overline{\left[u_i'\left[p' + \frac{\overline{\rho}\,u_j' u_j'}{2}\right]\right]} + \overline{\rho}\,\overline{u_1' u_3'}\frac{\partial \overline{u}_1}{\partial x_3} = \overline{\rho}\,J_b - \overline{\rho}\,\varepsilon. \quad (4)$$

The terms represent (from left to right) the rate of change of TKE, its transport by pressure-work terms and triple correlations; TKE production by downgradient momentum transport ($-\overline{\rho u_1' u_3'}$) in a mean shear flow; the loss of TKE associated with the raising of mean potential energy due to the buoyancy flux J_b, and the loss of TKE to dissipation by molecular viscosity.

The turbulence examined here is probably forced by a combination of low-frequency shear and internal waves, and is consequently highly intermittent. The intermittent nature of the forcing means that the TKE production term in (4) is not strictly correct, there being no steady shear related to the production. We will regard the production term in (4) as representing the average rate of energy conversion from the internal wave field to turbulence. Our observations consist of a spectrum of overturns with a range of length scales and Reynolds numbers, and the resulting turbulent ''patches'' are at different temporal stages in their evolution. The underlying intermittency can be seen in several of the figures.

If the turbulence is statistically steady and homogeneous, then (4) reduces to

$$\overline{\rho}\,\overline{u_1' u_3'}\frac{\partial \overline{u}_1}{\partial x_3} = \overline{\rho}\,J_b - \overline{\rho}\,\varepsilon, \quad (5)$$

where

$$J_b \equiv -\frac{g}{\rho}\overline{\rho' w'} = -K_\rho N^2$$

is the vertical buoyancy flux[2] with N^2 defined as the segment average of $-g\rho_z/\overline{\rho}$ and

$$\varepsilon = \overline{\nu\frac{\partial u_i'}{\partial x_j}\left(\frac{\partial u_i'}{\partial x_j} + \frac{\partial u_j'}{\partial x_i}\right)} \approx \frac{15}{2}\nu\overline{\left(\frac{\partial u'}{\partial z}\right)^2}$$

is the rate of TKE dissipation (the approximation is valid if the turbulence is isotropic), and ν is the coefficient of molecular viscosity. In practice, ε is based on an average of the shear measured by two probes; these may be oriented parallel to one another (as was done on the *Hudson* cruise in spring 1993) or perpendicular to one another (as on the *Oceanus* cruise in fall 1992). If the flux Richardson number R_f is defined as the fraction of the turbulent energy source used to change the potential energy through buoyancy flux

$$R_f = J_b/\overline{u_1' u_3'}\frac{\partial \overline{u}_1}{\partial x_3}, \quad (6)$$

then the buoyancy flux can be estimated as a proportion of the dissipation ε, giving an estimate of the eddy diffusivity for density K_ρ (Osborn 1980)

$$K_\rho \equiv \frac{-J_b}{N^2} = \Gamma_t\frac{\varepsilon}{N^2}. \quad (7)$$

The proportionality factor $\Gamma_t = R_f/(1 - R_f)$ is often called the ''turbulent mixing efficiency,'' which is a misnomer since it is actually the ratio of buoyancy flux to dissipation.

Laboratory experiments (Linden 1979; Rohr et al. 1988) suggest that the flux Richardson number (and hence Γ_t) is a function of the gradient Richardson number $N^2[\partial\overline{u}/\partial z]^{-2}$, a measure of the intensity of forcing. Since forcing and dissipation must be linked, one might expect that R_f is also a function of the dimensionless dissipation $\varepsilon/(\nu N^2)$. In oceanic applications of the dissipation method, Γ_t is often taken to be close to the maximum observed value of about 1/4.

c. Dissipation coefficient: Γ_d

Oakey (1985) estimated the turbulent mixing efficiency Γ_t by forming the ratio of thermal and TKE dissipations

$$\Gamma_d \equiv \frac{\chi N^2}{2\overline{T}_z^2\varepsilon}. \quad (8)$$

In a turbulent, non-double-diffusive ($R_\rho > 7$) oceanic mixed layer, Oakey measured a mean mixing efficiency of 0.265 (with the 68% confidence region for the sample mean lying between 0.066 and 0.436).[3] Hamilton et al. (1989) call this quantity the ''scaled dissipation ratio,'' and Moum (1996) suggests that it be called the dissipation flux coefficient. In any case, Γ_d is an observed quantity distinct from Γ_t and they are only expected to be equal if

- the observed mixing is ''conventional'' high Reynolds number turbulence (so that $K_T = K_\rho$);
- the conditions for validity of both the Osborn–Cox (1972) and the Osborn (1980) models are satisfied.

We will use the term ''dissipation coefficient'' for Γ_d but, because of its historical usage, we also refer to it as the ''apparent mixing efficiency.''

d. Gargett's low Reynolds number scaling

Gargett (1988b) has proposed a pair of deterministic scalings for buoyancy-modified turbulence, which provide order of magnitude estimates of the turbulent mixing efficiency and its variation with turbulent intensity. Gargett's scalings differentiate between ''conventional'' high Reynolds number turbulence, isotropic between

[2] We define $K_\rho \equiv -J_b/N^2$.

[3] In fact, Oakey (1985) used $\Gamma_d = g\alpha(\frac{1}{3} \pm \frac{1}{6})\chi/\varepsilon\overline{T}_s$, which assumes that the stratification is predominantly thermal.

buoyancy and dissipation scales, and what she terms ''low vertical Reynolds number'' turbulence, for which buoyancy effects cause anisotropy at all scales. Both scalings assume that the Froude number $\mathrm{Fr} \equiv U/Nl$ is of $O(1)$, and that the Peclet number $\mathrm{Pe} \equiv Ul/\kappa \gg 1$, where the horizontal and vertical velocity scales of the largest turbulent ''eddies'' are taken to be U and W, and the corresponding length scales are l and h. The difference between the two scalings enters in the assumptions made about the size of the ''vertical'' Reynolds number, $\mathrm{Re}_w = Wh/\nu$. For the high Reynolds number scaling ($\mathrm{Re}_w \gg 1$) Gargett finds

$$U \sim W \sim \sqrt{\varepsilon/N}$$
$$l \sim h \sim \sqrt{\varepsilon/N^3}. \tag{9}$$

Thus, in the high Re_w case the turbulence is approximately isotropic. However, if the Reynolds number based on the horizontal length and velocity scales is large, but $\mathrm{Re}_w = O(1)$, very different vertical scales are predicted;

$$W \sim \sqrt{\nu N}$$
$$h \sim \sqrt{\nu/N}, \tag{10}$$

with horizontal velocity and length scales again given by (9). Thus, for $\mathrm{Re}_w \sim 1$ all scales are modified by the stratification, and the largest turbulent eddies are significantly anisotropic. Using values appropriate for the NATRE area ($\varepsilon \sim 1 \times 10^{-9}$ W kg^{-1}, $N \sim 4 \times 10^{-3}$ s^{-1}), we find that $U \sim 0.5$ mm s^{-1}, $l \sim 0.1$ m, $W \sim 0.05$ mm s^{-1}, and $h \sim 2$ cm.

If the turbulence is high Reynolds number and isotropic, then the molecular diffusivity of the stratification should not affect the turbulent fluxes. Then K_ρ and K_T should be equal, and combining (7) and (3) we find $\Gamma_d = \Gamma_t$. Since the molecular diffusivity of the stratifying component (heat or salt) should not affect the turbulent fluxes in this case, we expect that Γ_d should not be a function of R_ρ, and because the Reynolds number is assumed to be large, we would expect that Γ_d should not depend on the buoyancy Reynolds number $\varepsilon/(\nu N^2)$ either.

In the low Re_w case Gargett (1988b) predicts

$$\Gamma_t \approx (\varepsilon/\nu N^2)^{-1}, \tag{11}$$

implying a generally small mixing efficiency. Gargett's low Re_w scaling suggests that the scaled dissipation $\varepsilon/\nu N^2$ is a measure of the anisotropy of the turbulent eddy field, and of the (inverse) mixing efficiency, whereas for high Re_w, $\varepsilon/\nu N^2$ is best thought of as a (buoyancy) Reynolds number.

The scaling arguments in Gargett (1988b) were based on the assumption that the Peclet number is large, so that even at low vertical Reynolds number, small-scale stirring should dominate over molecular diffusion as a mechanism for incorporating entrained fluid parcels into their surroundings. If this is the case, then the turbulence ''does not care'' what the stratifying agent is. Gargett's assumption was apparently motivated by laboratory experiments in which salt (which has a rather low diffusivity) was the stratifying property. However, if temperature makes an important contribution to the stratification, then the thermal Peclet number is

$$\mathrm{Pe}_T \equiv \frac{Wh}{\kappa_T} = \frac{\nu}{\kappa_T}\mathrm{Re}_w, \tag{12}$$

and the salt haline Peclet number is

$$\mathrm{Pe}_S \equiv \frac{Wh}{\kappa_S} = \frac{\nu}{\kappa_S}\mathrm{Re}_w, \tag{13}$$

where κ_T and κ_S are the molecular diffusivities of heat and salt. Thus, if $\mathrm{Re}_w \sim 1$, then $\mathrm{Pe}_T \sim 7$ and $\mathrm{Pe}_S \sim 500$, so the thermal Peclet number may not be very large, and one might expect to see a Pe dependence like that observed by Turner (1968) for interfacial entrainment. Gargett (1988a) alludes to this possibility, noting that heat and salt could mix unequally.

e. Salt finger mixing

The unstable ''salty on top'' stratification in the NATRE area provides a source of potential energy that can be released by salt fingers (Turner 1973). Hamilton et al. (1989) suggest that, if mixing due to salt fingers dominates that due to turbulence, then (4) reduces to

$$J_b = \varepsilon, \tag{14}$$

and K_T is again given by (3). This allows derivation of a formula for the dissipation coefficient Γ_d, given a salt finger buoyancy flux ratio (γ_f)

$$\Gamma_d = \frac{\gamma_f(R_\rho - 1)}{R_\rho(1 - \gamma_f)}. \tag{15}$$

Hamilton et al. (1993) observed large values of Γ_d (with median values of about 0.5) in data from beneath the core of Meddy ''Sharon,'' and invoked salt fingers to explain the elevated Γ_d values.

The model of McDougall and Ruddick (1992) can be used to quantify mixing rates due to the combined effects of both salt fingers and turbulence, provided the flux ratio of the salt fingers and the mixing efficiency of the turbulence is known. For the model to be used, Γ_d must lie between Γ_t and the finger values given by (15), so that the relative position between these values can be used to apportion the mixing between turbulence and fingers.

In section 4 we compare Γ_d with the values and behavior predicted by the three hypotheses discussed in section 2. The expected functional behavior of $\Gamma_d(R_\rho, \varepsilon/\nu N^2)$ under each of these hypotheses is summarized in Table 1.

TABLE 1. Expected behavior of Γ_d according to different mixing models.

	Isotropic turbulence	Anisotropic turbulence	Salt fingers	SF and turbulence
$\Gamma_d\ (R_\rho)$	independent	may vary	varies [Eq. (15)]	varies [between Γ_t and Eq. (15)]
$\Gamma_d\left(\frac{\varepsilon}{\nu N^2}\right)$	Const., $O(1)$	$<O(1)$, -1 slope	N.A.	?

3. Turbulence observations

a. Field observations

After the injection cruise in April 1992, two NATRE cruises were devoted to sampling the tracer and simultaneously observing turbulent microstructure with EPSONDE and its twin, ELITESONDE. The first was on the RV *Oceanus* in fall 1992 (26 Oct–19 Nov 1992) and the second was on the CSS *Hudson* in spring 1993 (5 Apr–14 May 1993). Over 800 profiles to depths of about 360 m were obtained on the fall cruise and nearly 1000 were taken during the spring cruise, giving detailed measures of temperature and velocity microstructure on cm scales, and of CTD parameters (conductivity, temperature, and pressure) on scales of order 1 m. The typical sampling routine involved a CTD cast, tracer samples at selected depths chosen relative to the target isopycnal, followed by a series of EPSONDE microstructure profiles. Figure 1 shows the tracer release site, the location of the tracer during the fall 1992 and spring 1993 cruises (Ledwell et al. 1993, 1994) and the locations of the EPSONDE stations. The coincidence of the microstructure observations and tracer ensures that the turbulent diffusivity estimates are representative of the tracer plume; however, the microstructure was sampled over about 3 weeks in fall 1992 and for nearly six weeks in spring 1993, while the tracer was affected by mixing processes during the entire experiment.

Composite profiles of temperature, salinity, and density ratio (R_ρ) calculated over 8-m segments are shown in Fig. 2. Individual 8-m averages are shown as points, and depth-bin-averaged profiles as solid lines. Depth-bin averages of R_ρ were[4] computed as $\langle \alpha T_z \rangle / \langle \beta S_z \rangle$, and only data segments for which the gradients T_z and S_z were uncertain by less than 25% were used. The temperature and salinity are (on average) stratified in the salt fingering sense. There was a mixed layer in the upper 60 m of the water column during the fall 1992 cruise, whereas the spring 1993 cruise showed a surface mixed layer of ~90 m, with a remnant winter mixed layer base at ~170 m. The spring 1993 cruise covered a much wider geographical area than the fall cruise, accounting for the larger variation of water properties. It is also possible that some of the salinity variation apparent in the spring profiles may be due to conductivity sensor calibration errors, but these have little or no effect on gradient quantities such as Γ_d, R_ρ, and $(\varepsilon/\nu N^2)$, which are our primary interest. A strong vertical variation in density ratio is evident, going from a nearly uniform value of 1.6 below 150 m to more variable and larger within the mixed layer. The upper mixed layer for the fall 1992 cruise was stably stratified in both T and S (negative density ratio).

b. Diffusivity from temperature microstructure: The Osborn–Cox model

We now examine the turbulent diffusivity inferred from temperature microstructure via the Osborn–Cox (1972) model. Figure 3 shows the depth-bin-averaged temperature gradient, thermal dissipation (χ), and turbulent diffusivity K_T for each cruise. Only data segments for which T_z was uncertain by less than 25% were used to compute the average profiles of T_z and K_T. Because the appropriate method for computing averages of microstructure quantities like χ and ε is unclear (e.g., Baker and Gibson 1987; Davis 1996), we show both arithmetic averages (filled circles) and maximum likelihood estimates (MLE, see the appendix). The method of averaging appears to have little effect on the profiles. Bin averages of χ computed using the MLE for lognormal variables are shown as solid curves, with shading giving 95% confidence intervals, and arithmetic means are shown as filled circles. Bin averages of K_T were computed using the MLE estimator to give

$$\left\langle \frac{\chi}{2T_z^2} \right\rangle$$

(solid curve with shading) and averages computed as $0.5\langle\chi\rangle/\langle T_z\rangle^2$ are shown as filled circles. The temperature gradient exhibits a maximum near the mixed layer base for each of the cruises, and depth profiles of χ tend to mimic T_z. The diffusivity K_T is quite large and variable, and more uncertain near the surface, primarily due to small and highly variable temperature gradients at these depths. Below the mixed layer the diffusivity is well estimated and has small estimated uncertainty.

Below the mixed layer the diffusivities estimated for the spring and fall cruises are of the order of 10^{-5} m^2 s^{-1}, and there are significant differences between the

[4] The notation $\langle \cdot \rangle$ denotes an average. For gradient quantities like T_z and S_z a simple arithmetic mean is used, while for microstructure quantities $\langle \cdot \rangle$ may refer to either an arithmetic average or an MLE estimate (see the appendix).

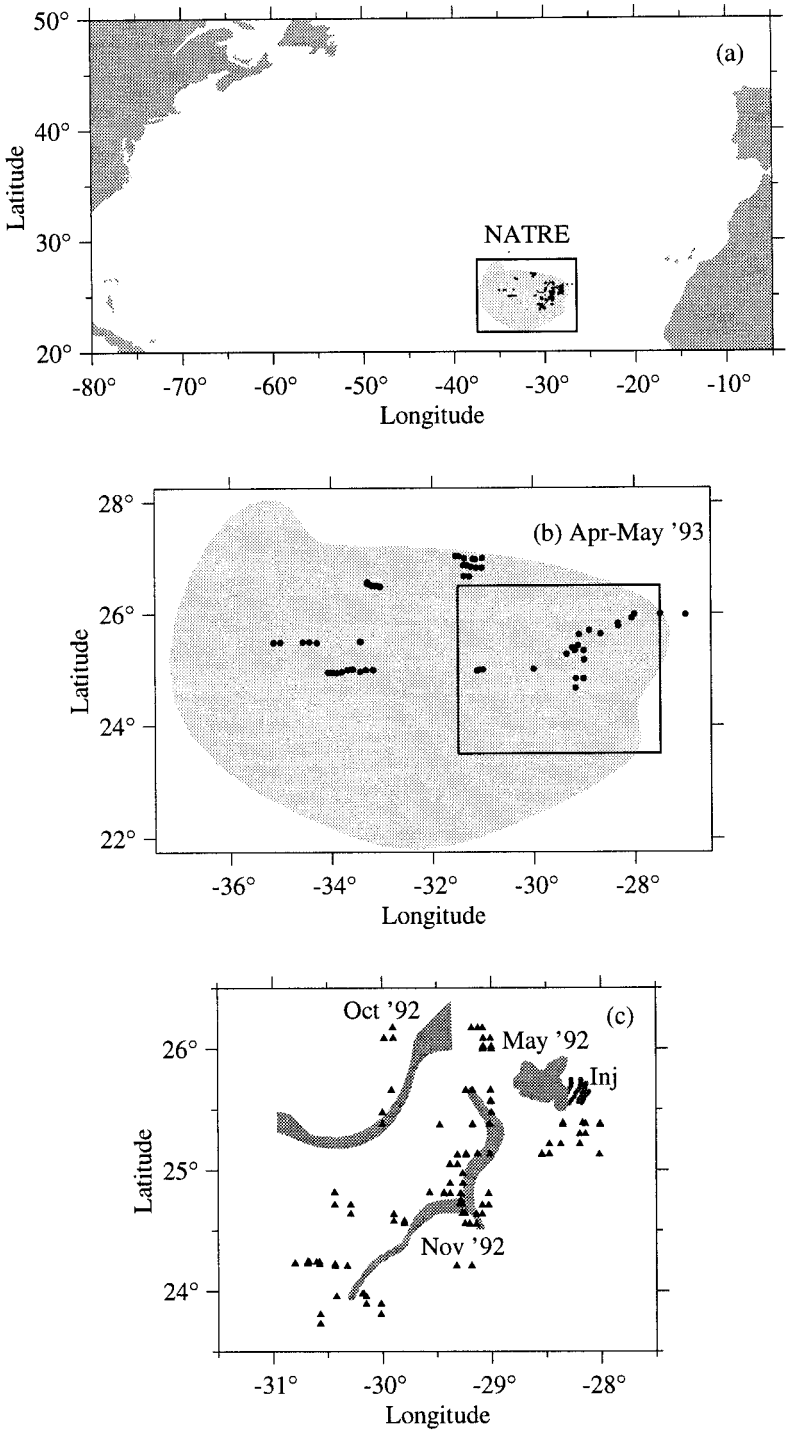

FIG. 1. Map showing the location of the NATRE experiment (panel a). Panel b is an enlargement of the NATRE survey region, with the shading showing the area in which significant quantities of dye were found during the cruise in April and May 1993 on the CSS *Hudson* (adapted from Clark 1997). Filled circles (●) mark the locations of the microstructure profiles that were taken. Panel c is an expanded view of the boxed area in panel b, showing the locations of the initial injection in spring 1992 and the dye streaks that were mapped out in three subsequent cruises (adapted from Ledwell et al. 1993). The microstructure profiles taken from the RV *Oceanus* during October and November 1992 are shown as filled triangles (▲).

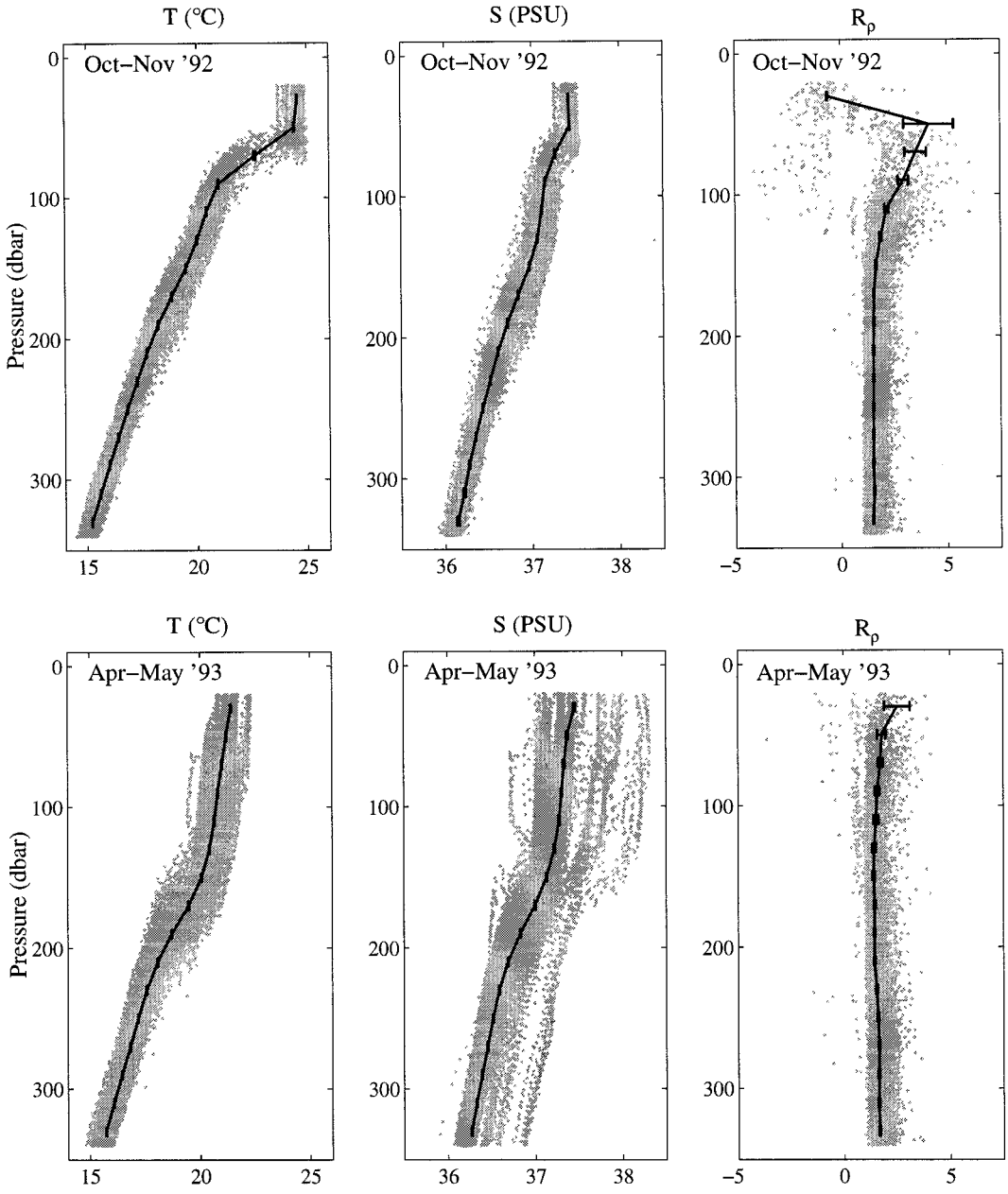

FIG. 2. Vertical profiles of T, S, and R_ρ taken during cruises on the RV *Oceanus* in fall 1992 (top three panels) and on the CSS *Hudson* in spring 1993 (bottom panels). Individual measurements are scatterplotted in gray. The data were divided into 20-m depth bins, and bin averages computed; solid curves show computed bin averages with error bars giving the estimated 95% confidence intervals. In the right-hand panels, only data from segments with estimated gradient uncertainties of less than 25% are shown.

spring and fall observations. In the fall, the diffusivity is nearly uniform at these depths, with values of $\sim 1 \times 10^{-5}$ m^2 s^{-1}, while in the spring the diffusivity was significantly larger, ranging from 2×10^{-5} m^2 s^{-1} at 300 m to 5×10^{-5} m^2 s^{-1} at 100 m. These differences do not appear to be due to geographical variations in K_T associated with the greater geographical extent of the spring 1993 survey, as little lateral variation is apparent in either the fall or spring data. The substantially larger diffusivity observed at depth in the spring is consistent with the tracer studies of Ledwell et al. (1993) and Ledwell and Watson (1994), who found the average diffusivity for the winter months to be roughly twice as large as that for the summer months. The diffusivity estimated from the vertical spread of the tracer over the previous six months is shown as an open box. The height of each box indicates the depth range over which the tracer concentration was >50% of its peak value at the

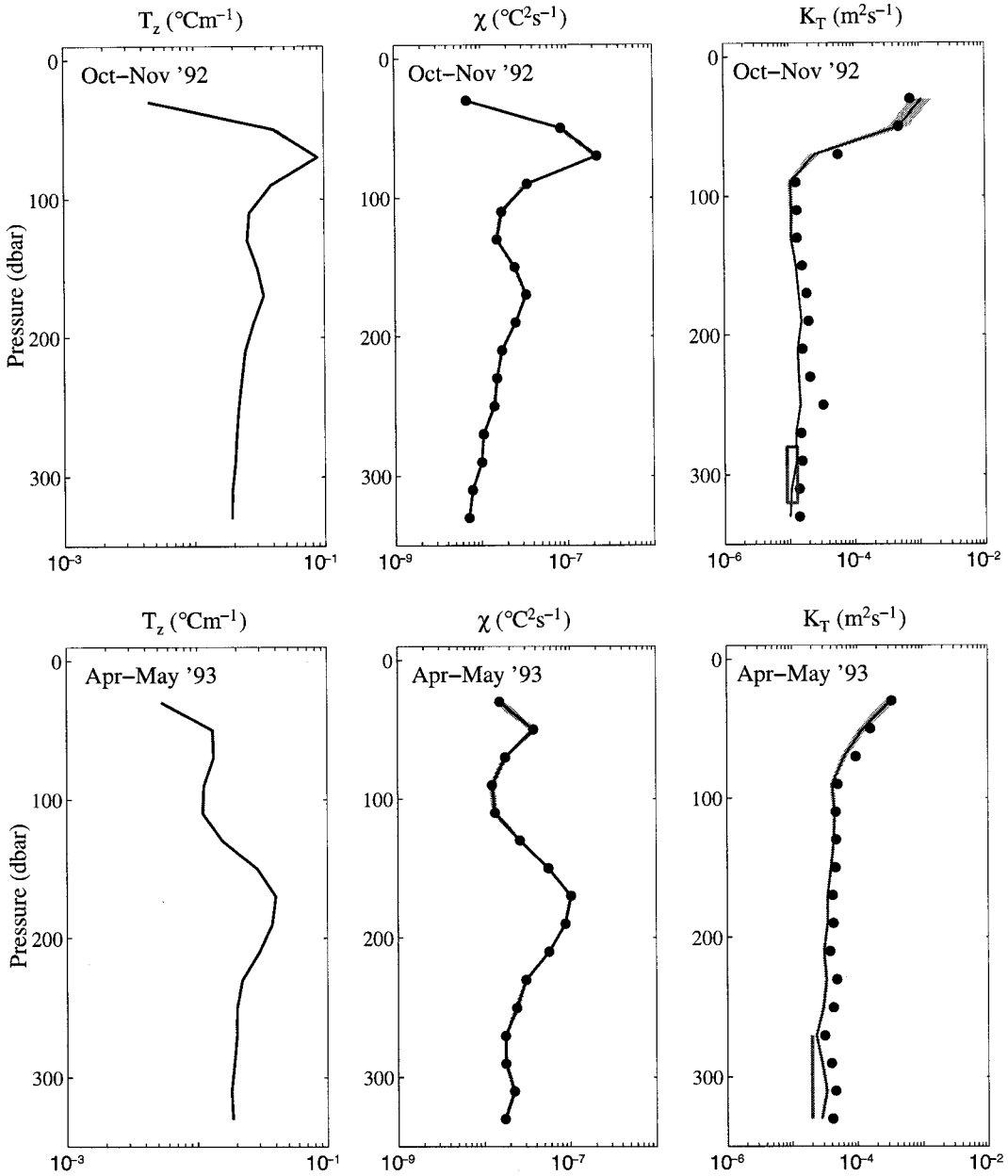

FIG. 3. Vertical profiles of temperature gradient (T_z), thermal dissipation (χ), and thermal diffusivity (K_T) from cruises on the RV *Oceanus* in the fall of 1992 (top three panels) and on the CSS *Hudson* in spring 1993 (bottom panels). The data were divided into 20-m depth bins, and bin averages were computed. Shading shows the estimated 95% confidence intervals on the bin averages, which are shown as solid curves. For χ, bin averages were computed using a MLE for lognormally distributed quantities (see the appendix), and the corresponding arithmetic means are shown as filled circles. For K_T, the solid curves show bin averages of $K_T = 0.5\chi/T_z^2$, and the filled circles show bin averages computed as $K_T = 0.5\langle\chi\rangle/\langle T_z\rangle^2$. The shaded boxes at ~300 m show the diffusivity inferred from dye measurements, with the height of each box giving the vertical extent of the dye.

time of the sampling cruise, and the width of each box indicates the estimated uncertainty of the tracer-derived diffusivity (where available). The tracer and microstructure-derived diffusivities are in good agreement.

The histograms and probability plots of χ, ε, and Γ_d that follow (Figs. 4–6) are for the depth range 240–340 m that brackets the tracer, over which conditions are more uniform than in the upper 240 m. The probability distribution function (PDF) of logχ for the depth range are shown as histograms (Figs. 4a,c) and probability plots (Figs. 4b,d). The axes of the probability plot are such that a lognormally distributed variate would yield a straight line, with a steeper slope signifying a narrower distribution. The straight lines in panels b and d rep-

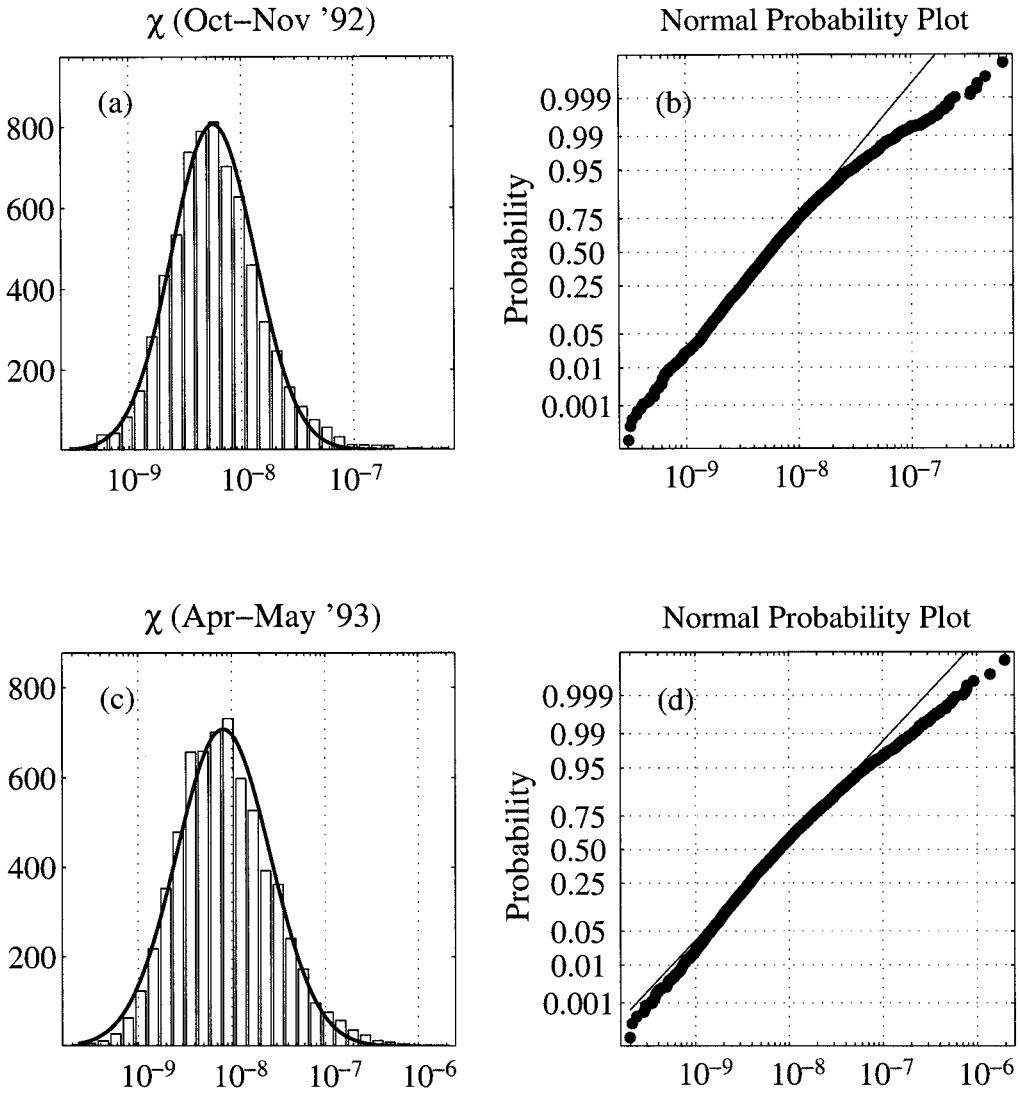

FIG. 4. Histograms and normal probability plots of log χ for the depth range 240–340 m. The histograms in panels (a) and (c) show data from the fall 1992 and spring 1993 cruises, respectively, and the corresponding probability plots are shown in panels (b) and (d). The solid curve superimposed on the histograms shows the best-fit lognormal distribution, which was obtained by fitting to the central 50% of the distribution. For the fall cruise, log χ has a mean of -8.25, a standard deviation of 0.37, and the MLE-estimated mean of χ is $8.1(\pm 0.2) \times 10^{-9}$ °C^2 s^{-1} (uncertainties represent 95% confidence intervals); for the spring cruise log χ has a mean of -8.09, a standard deviation of 0.50, and the MLE-estimated mean of χ is $1.6(\pm 0.06) \times 10^{-8}$ °C^2 s^{-1}.

resent a linear least squares fit to the central 50% of the distribution, and the corresponding ''best fit'' distributions are shown by the solid curves in panels a and c. The plots show that χ is approximately lognormal, although both cruises show a moderate excess of large values relative to the central 50% of the distribution. The MLE-estimated mean of χ for the fall 1992 data (240–340 m) is $8.1(\pm 0.2) \times 10^{-9}$ °C^2 s^{-1}, while for the spring 1993 data it is $1.6(\pm .06) \times 10^{-8}$ °C^2 s^{-1}—a factor of 2 larger. The corresponding values of K_T for the 240–340-m depth range are $1.0(\pm 0.04) \times 10^{-5}$ m^2 s^{-1} and $2.2(\pm 0.1) \times 10^{-5}$ m^2 s^{-1} for the fall and spring cruises, respectively. The computed MLE estimate of $\langle \chi \rangle$ for the two cruises is $1.1(\pm 0.02) \times 10^{-8}$ °C^2 s^{-1}, and $\langle T_z \rangle = 1.9(\pm 0.01) \times 10^{-2}$ °C/m (using only segments with estimated gradient errors $< 25\%$), so that $\langle K_T \rangle = 1.5(\pm 0.05) \times 10^{-5}$ m^2 s^{-1} for the depth range 240–340 m, in agreement with the tracer observations, and with the microstructure-inferred diffusivity of 1.4×10^{-5} m^2 s^{-1} reported by Sherman and Davis (1996). We note that the values of $\langle \chi \rangle$ (and the corresponding K_T values) quoted here are somewhat smaller than those apparent in Fig. 3 for the same 240–340-m depth range. The reason for this is that only the central 50% of the distribution is used here, whereas all χ values within a depth bin were used to generate the profiles in Fig. 3. The slight

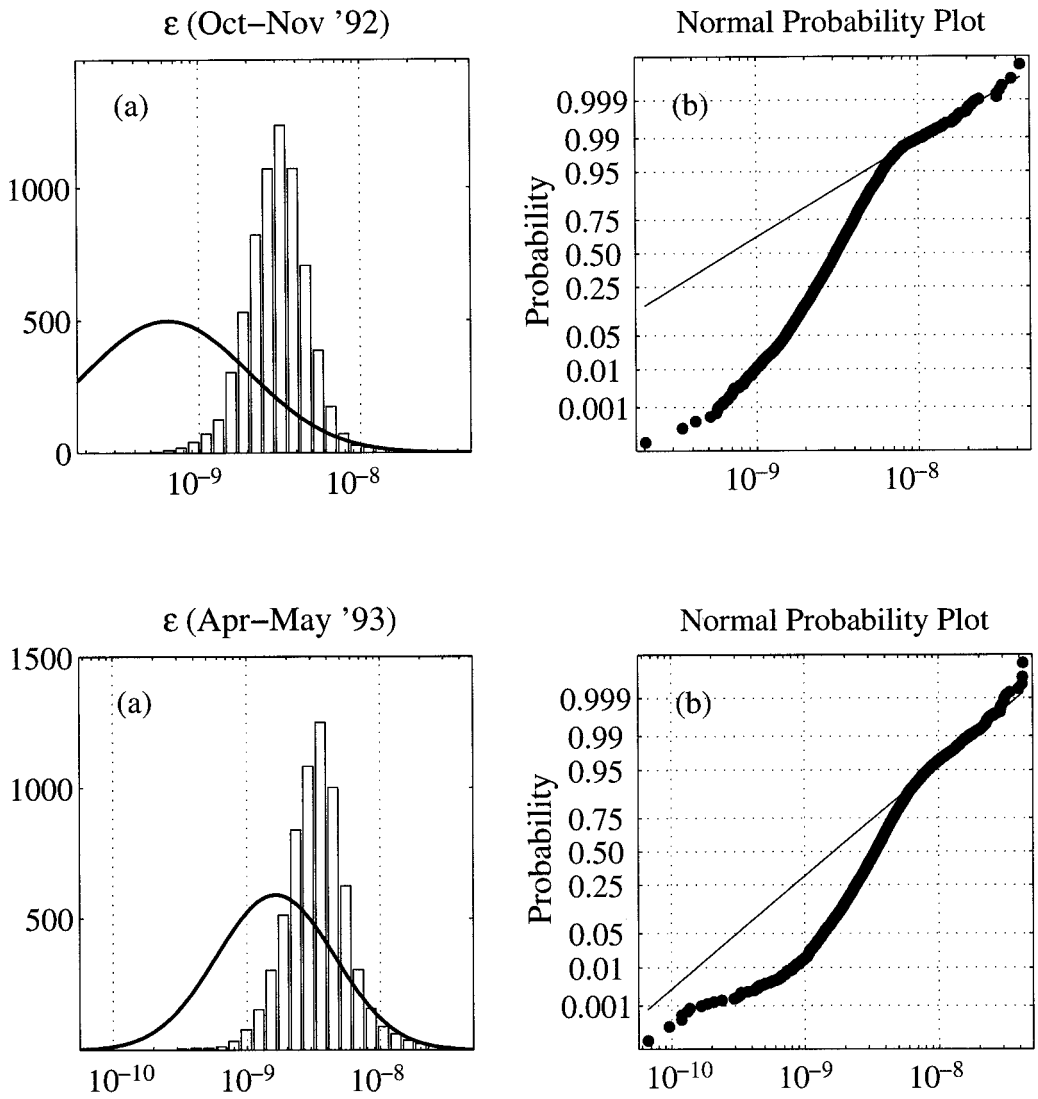

FIG. 5. Histograms and normal probability plots of the turbulent kinetic energy dissipation rate (ε) for the depth range 240–340 m. The histograms in (a) and (c) show data from the fall 1992 and spring 1993 cruises, respectively, and the corresponding probability plots are shown in (b) and (d). The solid curves superimposed on the histograms show the best-fit lognormal distributions for the upper tail of the distributions ($\varepsilon > 7.0 \times 10^{-9}$ W kg^{-1}, and excluding the upper 0.1% of the distribution). For the fall cruise, the extrapolated distribution has a logarithmic mean of -9.2, a logarithmic standard deviation 0.51, and the MLE-estimated mean of ε is 1.26×10^{-9} W kg^{-1}; for the spring cruise the extrapolated distribution has a logarithmic mean of -8.79, a logarithmic standard deviation of 0.44, and the MLE-estimated mean of ε is 2.75×10^{-9} W kg^{-1}.

"excess" of large χ values apparent in Fig. 4 leads to slightly larger computed means for the depth profiles.

c. Velocity microstructure

Temperature microstructure and the Osborn–Cox (1972) model suggest a diapycnal diffusivity of 1.5×10^{-5} m^2 s^{-1}. If this mixing is achieved by turbulence with an efficiency of 0.265, then the observed mean value of N of 4.0×10^{-3} s^{-1} for the depth range 240–340 m leads us to expect a mean dissipation rate of turbulent kinetic energy, $\langle\varepsilon\rangle \approx 1.0 \times 10^{-9}$ W kg^{-1}. The lognormal distribution of temperature dissipation leads us to expect a lognormal distribution of ε of similar width. Histograms of TKE dissipation (Figs. 5a,c) show a narrow distribution (with logarithmic standard deviation of 0.17–0.20) centered about 3×10^{-9} W kg^{-1}. The MLE-estimated means of the measured dissipation are 3.3×10^{-9} W kg^{-1} and 3.7×10^{-9} W kg^{-1} for the fall and spring cruises, respectively, several times larger than expected. The probability plots (Figs. 5b,d) show two straight regions, suggesting a bimodal distribution, the first of these lies between 10^{-9} and 7×10^{-9}, and the second falls between 7×10^{-9} and 2–3 ($\times 10^{-8}$).

The first region corresponds to the large narrow peak in the histograms, while the second corresponds to the extended tail of higher dissipation values. The straight solid line shown on the probability plots corresponds to the solid curves on the histograms, representing a log-normal distribution with a logarithmic mean of -9.2 and logarithmic standard deviation of 0.51 for the fall cruise, and a logarithmic mean of -9.79 and a logarithmic standard deviation of 0.44 for the spring 1993 cruise. These curves, derived from the tail of the observed distributions, are consistent with what we expect from the temperature and tracer observations. The observations of ε are therefore consistent with an underlying broad distribution centered on roughly 10^{-9} W kg^{-1}, upon which a narrow noise distribution centered on 3×10^{-9} W kg^{-1} is superposed. The extrapolated distributions suggest a mean ε of 1.26×10^{-9} W kg^{-1} for the fall 1992 cruise, and a mean of 2.75×10^{-9} W kg^{-1} for the spring 1993 cruise. Taken together with Fig. 4, this suggests that both χ and ε were larger by a factor of 2 to 3 during the spring 1993 cruise.

To obtain an estimate of the instrumental noise in ε as a function of drop speed, EPSONDE was dropped repeatedly in a quiescent seawater-filled tank of diameter 3 m and depth 10 m. A noise level of roughly 1.5×10^{-9} W kg^{-1} was found to be associated with hydrodynamic noise from a sensor guard assembly (since redesigned). It was originally hoped that this noise could be subtracted, but the nonlinear nature of the problem and of the data analysis has precluded this. We have concluded that dissipation values less than 7.0×10^{-9} W kg^{-1} (this value corresponds to the intersection of the two straight-line portions of the probability plots) are likely to be contaminated by hydrodynamic guard noise, while values larger than this are not.

The contamination of the ε observations precludes direct estimation of $\langle\varepsilon\rangle$ and of $\langle K_\rho\rangle$ using the Osborn (1981) dissipation model. However, the dissipation coefficient Γ_d can be computed for data segments in which ε is large enough to be uncontaminated. The density and temperature gradient in each 8-m data segment were estimated by a linear least squares fit, and the gradient uncertainty was estimated from the residuals. Each 8-m data segment was required to pass the following four criteria in order to be included in the subsequent analysis:[5]

1) The shear and temperature gradient spectra must be visually consistent with the expected ''universal spectrum'' of Nasmyth (Oakey 1982). [48%]
2) The segment-averaged dissipation rate must exceed 7.0×10^{-9} W kg^{-1} to be considered free of contamination by hydrodynamic guard noise. [5.8%]
3) The segment-averaged density gradient must be uncertain by no more than 25%. The major uncertainty was not instrumental noise, but small-scale nonlinearities in the density profile. [18.2%]
4) The segment-averaged temperature and salinity gradients must be uncertain by no more than 25%. Again, the major uncertainty was due to small-scale nonlinearities in the profiles rather than instrumental noise. [29%].

The above criteria resulted in only 0.9% of the data records (738 in all) being used to study Γ_d. The gradient criteria are necessary to minimize the creation of bogus trends due to imperfect estimation of gradients. This effect will be discussed in detail in section 4.

In studying Γ_d variations, we have chosen to combine data from the two cruises, primarily to reduce the statistical uncertainties on our bin-averaged quantities. The data indicate a mixing efficiency of $0.14(\pm 0.02)$ for the fall (for the depth range 20–340 m) and $0.21(\pm 0.02)$ for the spring, suggesting that the more intense microstructure activity in the spring was associated with more ''efficient'' mixing. This is consistent with the dependence of Γ_d on buoyancy Reynolds number found in section 4c, given the larger dissipations observed in the spring.

It is possible that sampling only the high dissipations (criterion 2) could bias the results to certain (high energy) phases of turbulent events. If χ and ε evolve differently through the course of each event, the computed dissipation coefficient would be biased. The histogram and probability plot of Γ_d computed for those records are shown in Fig. 6. The dissipation coefficient is log-normally distributed, with an MLE-estimated mean of $0.18(\pm 0.015)$, and a (logarithmic) standard deviation of 0.41, both of which are consistent with the earlier findings of Oakey (1982). Thus, it appears that any such bias is not large enough to dominate the results.

In the next section, we will examine systematic *variations* of dissipation coefficient Γ_d with respect to buoyancy Reynolds number and density ratio, without focusing on its magnitude. We find trends in Γ_d that we believe are not due to the truncation of the dataset, since if Γ_d were independent of both density ratio and buoyancy Reynolds number, then restricting the analysis to high values of buoyancy Reynolds number could not by itself induce a trend.

4. Variations in apparent mixing efficiency Γ_d

The working hypothesis to be tested is that Γ_d is independent of buoyancy Reynolds number ($\varepsilon/\nu N^2$) and density ratio R_ρ. We find small but systematic variations of Γ_d with both quantities. However, as we have found our analysis technique to be sensitive to errors in estimation of microstructure and gradient quantities, we first describe the Monte Carlo procedure we devised to validate our results.

[5] The percentage of the segments passing each criterion for the depth range from 20 to 340 m is shown in square brackets.

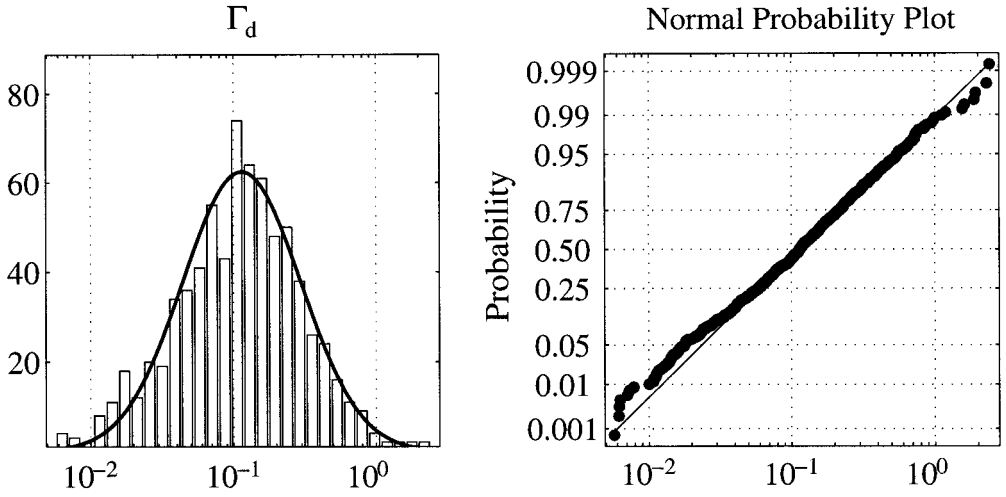

FIG. 6. Histogram and probability plot of the dissipation coefficient Γ_d, using data from both the fall 1992 and spring 1993 cruises. The data have been subsampled according to the criteria in section 3c. The solid curve in the left panel shows the best-fit lognormal distribution (corresponding to the solid curve in the right panel), which was obtained by fitting to the central 50% of the distribution. The fitted distribution has a logarithmic mean of -0.94, a logarithmic standard deviation of 0.41, and the MLE gives a value of $0.18(\pm 0.015)$ for the mean of Γ_d (uncertainties represent estimated 95% confidence intervals).

a. Effect of observational errors: Monte Carlo analysis of synthetic datasets

A serious problem of plotting derived quantities like Γ_d against R_ρ or $(\varepsilon/\nu N^2)$ is that measured quantities such as N^2 appear in all three variables. Therefore, random noise will appear in both the ordinate and the abcissa of the scatterplots. This could lead to apparent systematic variations of Γ_d with respect to either density ratio or buoyancy Reynolds number. To test the robustness of the trends we observe to sampling or observational errors in any of the quantities that make up Γ_d, we generated synthetic datasets and performed Monte Carlo tests on them. Several different artificial datasets were generated and tested, but our approach and overall results are well illustrated by the following one involving a synthetic TKE dissipation ε_s.

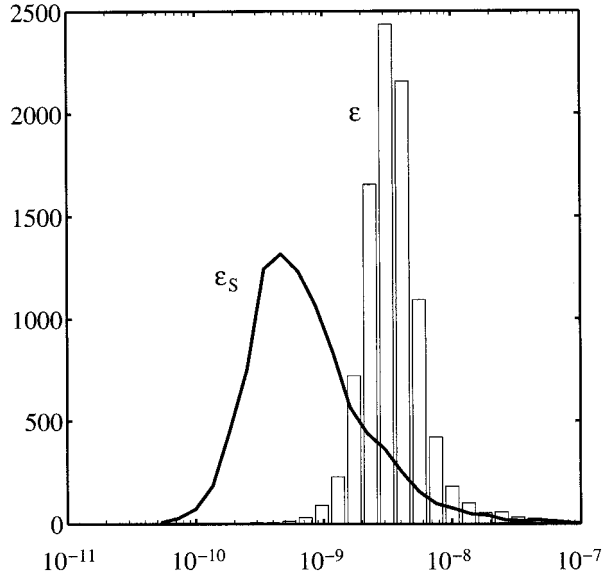

FIG. 7. Histograms of the measured dissipation rate (ε) and the synthetic dissipation data (ε_S) used in the Monte Carlo tests. The synthetic data were constructed so as to give a constant value of 0.265 for Γ_d. The measured dissipation ε has a mean of 4.1×10^{-9} W kg^{-1}, while the mean of the synthetic dissipation ε_S is 1.3×10^{-9} W kg^{-1}.

From each 8-m data segment, we constructed the synthetic dissipation (denoted by the subscript *s*) that would make the segment value of Γ_d equal to 0.265;

$$\varepsilon_s = \frac{1}{0.265}\frac{\chi N^2}{2T_z^2}. \tag{16}$$

Figure 7 shows the histograms of ε and ε_s. The synthetic dissipation has a broad lognormal distribution similar to what was expected, and the tail at high dissipation values matches the observed dissipation. In the sections that follow, we first examine the dependence of Γ_d on density ratio, using both observed and synthetic datasets, and then the dependence on buoyancy Reynolds number.

b. Γ_d versus R_ρ

Figure 8a shows segment-average values of Γ_d plotted against corresponding values of density ratio, for those records satisfying the criteria outlined in section 3 (acceptable spectra, dissipation rate exceeding the threshold value, gradient errors estimated at less than 25%). The maximum likelihood estimate (the appendix) of the bin-averaged Γ_d and the corresponding estimated 95% confidence intervals are shown by the solid curve and

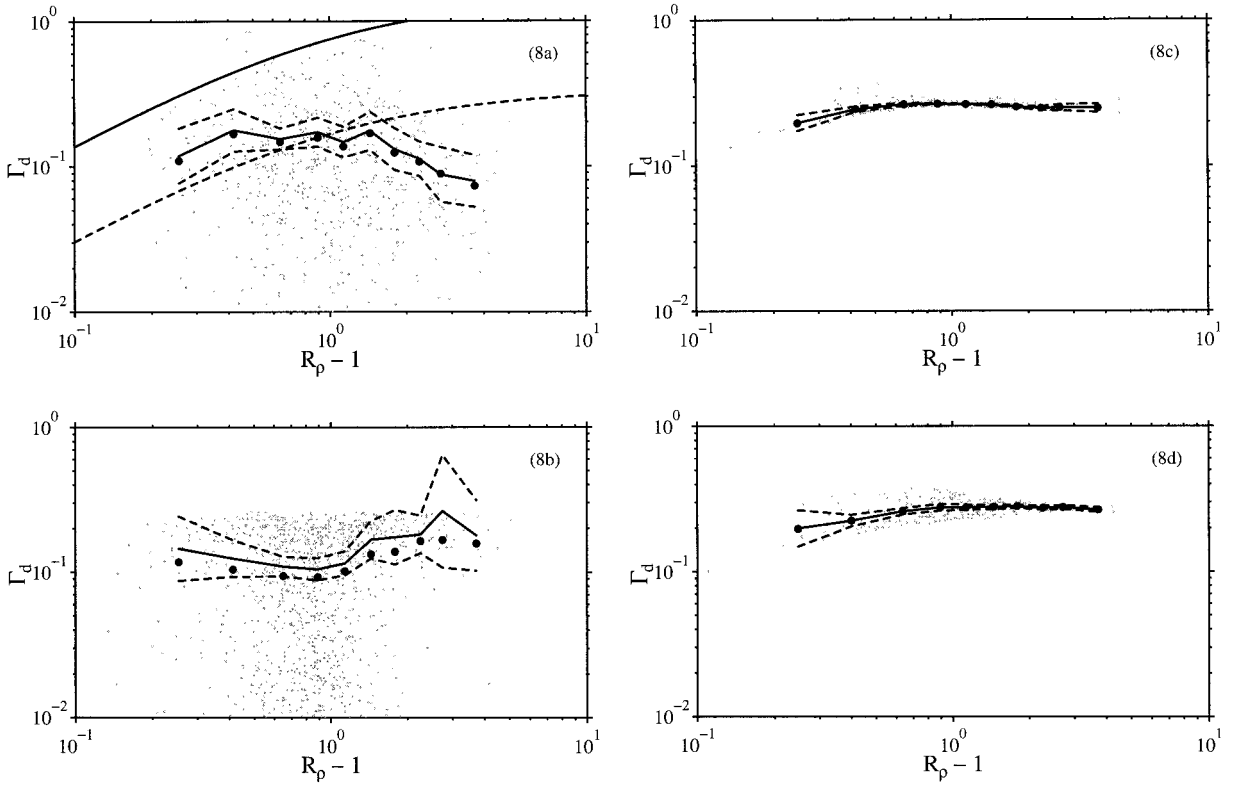

FIG. 8. The observed variation of the dissipation coefficient Γ_d with $(R_\rho - 1)$ (a). Solid curves show the MLE for the mean of Γ_d (with 95% confidence intervals shown by the dashed curves); filled circles show the corresponding arithmetic means. The additional curves in (a) show the expected behavior of Γ_d [from Eq. (15)] if the mixing were due to salt fingers with a flux ratio of 0.6 (solid curve) and 0.25 (dashed). (b)–(d) The results of Monte Carlo tests that were performed to see whether the observed trend in (a) could be reproduced by adding noise to observed quantities if Γ_d were independent of R_ρ. (b) The effect of adding noise with mean of 3×10^{-9} W kg^{-1} to ε_S. (c) and (d) The effect of 25% error in the estimation of temperature and salinity gradients, respectively.

shading, respectively. The arithmetic means are shown as open circles. A significant trend (in the sense of exceeding the computed error bars) is seen for R_ρ in the range 2.5–5. The solid and dashed curves show the apparent mixing efficiency computed from Eq. (15). The solid curve corresponds to a flux ratio of $\gamma_f = 0.6$, the value found experimentally by Schmitt (1979), while the dashed curve corresponds to $\gamma_f = 0.25$, the value predicted by the Howard and Veronis (1987) steady-state model. Although the observed behavior of Γ_d is roughly consistent with the dashed curve for low R_ρ, so that we cannot rule out fingers with a low flux ratio, the Monte Carlo tests below show that a more plausible explanation involves the effects of noise.

Figure 8b shows the same quantities, computed from the synthetic dataset altered by adding to ε_s a lognormally distributed random variate with mean and standard deviation corresponding to the narrow peak of Fig. 5 (logarithmic mean of -8.52, logarithmic standard deviation of 0.2); this corresponds to adding random noise with a mean value of 3×10^{-9} W kg^{-1}. The data were then sieved in the same manner as the observed data, and plotted as in panel a. The results confirm that noise in ε does not induce systematic dependence on density ratio.

Figure 8c shows the effect of adding random noise to temperature gradients consistent with the 25% error allowed by our sieving procedure. First, we computed a random variate whose logarithm was uniformly distributed between $(1.25)^{-1}$ and 1.25. This was multiplied by the temperature gradient to form[6] T_{zs}; N_s^2 was then computed from the ''noisy'' temperature gradient and the measured salinity gradient:

$$N_s^2 = g\alpha T_{zs} - g\beta S_z. \tag{17}$$

The noisy density ratio was similarly calculated:

$$R_{\rho s} = \alpha T_{zs}/\beta S_z. \tag{18}$$

This synthetic dataset was then sieved and plotted in the same manner as the original data. The result shows a weakly increasing trend in the density ratio range of

[6] The subscript s is used here to denote a synthetic ''noisy'' temperature gradient; similar notation is used for other gradient-derived quantities.

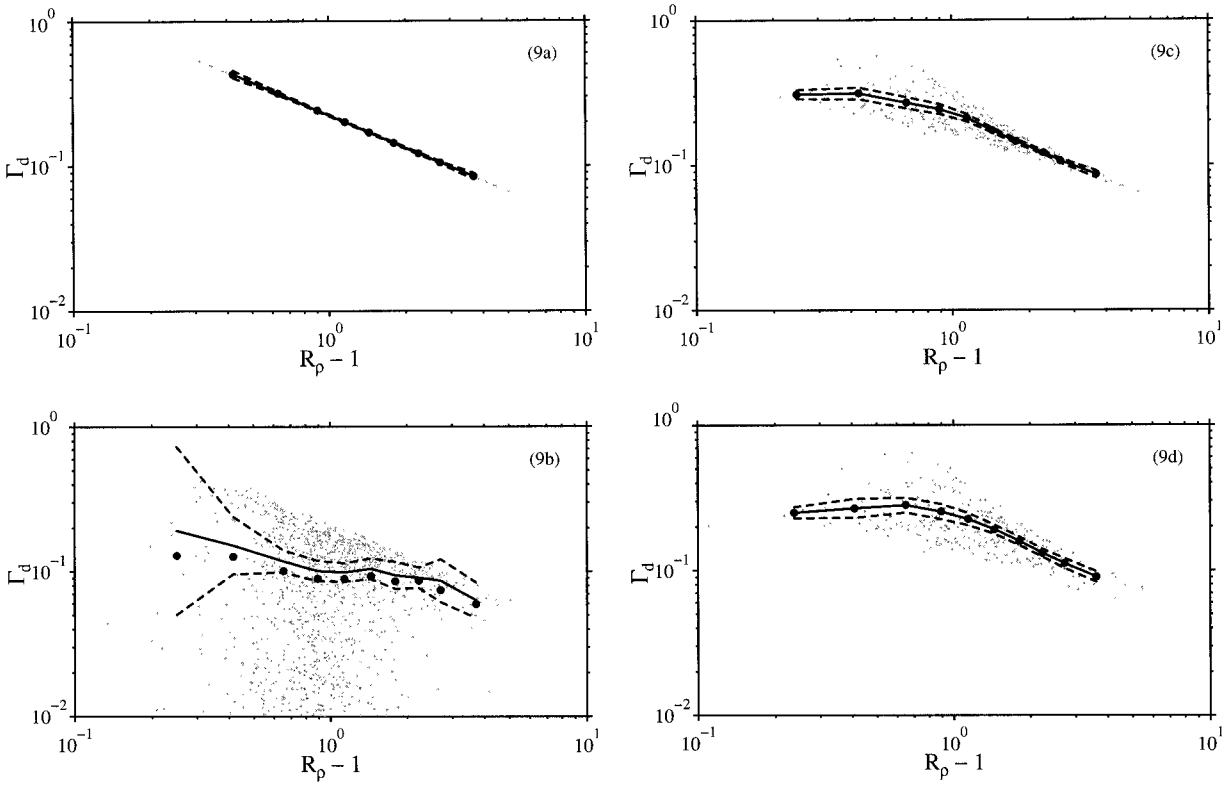

FIG. 9. Monte Carlo test designed to investigate the robustness of the decreasing trend observed in Fig. 8a at high values of R_ρ. (a) The decreasing trend exhibited by the synthetic dataset. (b) The effect of adding noise with mean of 3×10^{-9} W kg^{-1} to ε_S. (c) and (d) The effect of 25% error in the estimation of temperature and salinity gradients, respectively. The solid curves show the MLE for the mean of Γ_d (with 95% confidence intervals shown by the dashed curves); filled circles show the corresponding arithmetic means.

1–2, and no significant trend above that. Similar but slightly stronger trends are induced by 25% random noise in the salinity gradient, again linked to errors in the computed buoyancy frequency (Fig. 8d). The trends that are induced by noise in either the temperature or salinity gradients are inconsistent with those observed in panel a.

Our observations are broadly consistent with a negative dependence on density ratio that is cancelled in the range $1 < R_\rho < 2$ by the effects of noise on the estimated salinity or temperature gradients. This conclusion is further supported by increasing the temperature and salinity gradient error level to 50%, which causes a positive trend in the range $1 < R_\rho < 2.5$, and leaves the negative trend at larger R_ρ unchanged. The effect of a 50% salinity or temperature gradient noise level on synthetic data is to induce an increased positive trend in the range $1 < R_\rho < 2$, enhancing the convex dependence seen in Fig. 8a.

We conclude that the negative trend observed in Fig. 8a is real. The trend may in fact extend over the full observed range of density ratio, but the dependence is likely to be masked at low density ratio by errors in estimating the temperature or salinity gradient. To test this, we generated a new synthetic dataset, this time computing ε_s to give a decreasing trend similar to that observed in Fig. 8a over the full range of R_ρ. The resulting R_ρ dependence is shown in Fig. 9a. Panel b shows the effect of adding noise with a mean of 3×10^{-9} W kg^{-1} to the synthetic dissipations; panels c and d show the effect of 25% error in T_z and S_z—the procedure was identical to that discussed in connection with Figs. 8c, d. The plots in panels b, c, and d are similar to the actual dependence shown in Fig. 8a, consistent with the hypothesis of an overall decreasing trend which is masked at low R_ρ by noise.

c. Γ_d versus buoyancy Reynolds number

Figure 10 examines the dependence of Γ_d on buoyancy Reynolds number in the same manner as in Fig. 8. Figure 10a shows a significant increasing trend, with Γ_d increasing from 0.1 to about 0.35 as Re increases from 40 to 2000. Additive noise on ε (Fig. 10b) induces a very weak increasing trend for Re above 600 in the simulations. This trend is far too weak to explain the observed trend in panel a. Panels c and d show the effect of 25% noise in temperature and salinity gradients respectively; there is a very weak positive trend, inconsistent with the observed one. Experiments on datasets synthesized in different ways (not shown) also exhibited no induced trends consistent with those we observed.

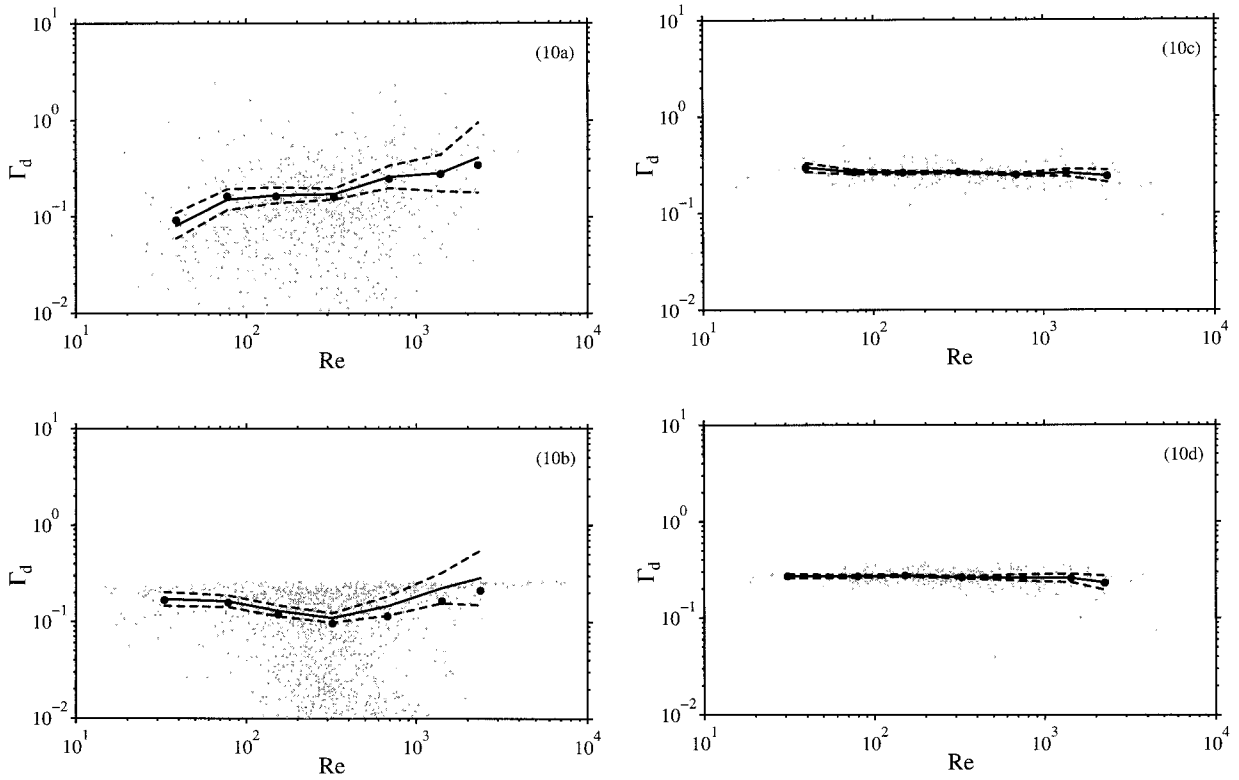

FIG. 10. Variation of dissipation coefficient Γ_d with turbulence activity parameter $\varepsilon/(\nu N^2)$ (a). The solid curves show the MLE for the mean of Γ_d (with 95% confidence intervals shown by the dashed curves); filled circles show the corresponding arithmetic means. (b), (c), and (d) The results of Monte Carlo tests designed to investigate whether the observed trend in (a) could be reproduced by adding noise to observed quantities if Γ_d were independent of $\varepsilon/(\nu N^2)$. (b) The effect of adding noise with mean of 3×10^{-9} W kg^{-1} to ε_S. (c) and (d) The effect of 25% error in estimation of temperature and salinity gradients, respectively.

We conclude that Γ_d exhibits a systematic increase with buoyancy Reynolds number that is not induced by measurement error.

The Monte Carlo tests have taught us a valuable lesson: Testing the hypothesis that Γ_d is independent of density ratio is very sensitive to noise in temperature or salinity gradients due to the consequences on estimated N^2. We tried to devise a statistically valid test that avoided plotting "x against x," but were unsuccessful. Monte Carlo simulations seem to be the best way to estimate the effects of noise on such results.

5. Discussion

The diffusivity obtained from thermal dissipation measurements and the Osborn–Cox model agreed well with that inferred from tracer observations, and show clear variations of K_T with depth and time. The velocity microstructure observations were contaminated by sensor guard noise such that we had to select relatively energetic 8-m data segments with dissipation rates exceeding 7×10^{-9} W kg^{-1} for our analysis. This precluded direct estimation of K_ρ using Osborn's dissipation model. However, the data segments in which ε was high enough to be uncontaminated were examined with respect to the dissipation coefficient Γ_d, to test for consistency with the mixing mechanisms proposed in section 2. Although selecting for high dissipation events (or parts of events) could lead to a bias in Γ_d, the histogram of Γ_d for the selected data (Fig. 6) suggests that any such bias is small. The potential problem of bias was minimized by focusing on *variations* of Γ_d rather than its magnitude.

Previous observations of Γ_d (Table 2) from a variety of locations by other observers find Γ_d ranging from 0 to 0.4. Our observations are well within this range. So far as we can determine, ours appears to be the first attempt to discern systematic variations of Γ_d with respect to dimensionless parameters such as density ratio. We found Γ_d to decrease systematically with increasing density ratio and to increase systematically with increasing buoyancy Reynolds number. Monte Carlo experiments show that the observed trends are not likely to have been induced by measurement errors. A comparison of our findings with the predictions of the hypothesized mixing mechanisms (Table 1) from section 2 shows the dependence of Γ_d to be not fully consistent with isotropic turbulence, low vertical Reynolds number turbulence, or salt fingers. Models involving salt fingers cannot explain the decreasing trend observed at large

TABLE 2. Summary of oceanic estimates of dissipation ratio. In the last column J_b is the buoyancy flux estimated by eddy-correlation techniques.

Reference	Location	R_ρ	$\varepsilon/\nu N^2$	Γ_d	$\Gamma_0 = \frac{J_b}{\varepsilon}$
Oakey (1982, 1985)	Rockall Trough	>7	300–3000	0.05–0.32	—
Peters et al. (1988)	Equatorial Pacific	~ -5	25–2500	0.1	—
Peters et al. (1985)	As above; spectra well resolved			0.1	—
Moum et al. (1989)	Equatorial Pacific	~ -5		0.11–0.32	—
Yamazaki and Osborn (1993)	Eastern N. Pacific, 42 m	~ -5	12–2500	—	0.05
Fleury and Lueck (1994)	Atlantic (12°N, 56°W) turbulent interface	1.6	85–480	0.003–0.14	0.01–0.28
Fleury and Lueck (1994)	Atlantic (12°N, 56°W) upper thermocline	∞	156–255	0.0–0.23	0.03–0.11
Fleury and Lueck (1994)	Atlantic (12°N, 56°W) T inversion	0.1	370–3200	—	0.05–0.12
Toole et al. (1994)	Eastern subtropical Atlantic, 2500–3000 dbar	~ 2	60	0.35	—
Gargett and Moum (1995)	Juan de Fuca Strait turbulent tidal flow	—	—	0.2 if $K_\rho > 0$ 0.13 if $K_\rho < 0$	0.63 if $K_\rho > 0$ -1 if $K_\rho < 0$
Moum (1996)	Midlatitude Pacific thermocline	—	—	0.3–0.4	0.15–0.2
Farmer (1975)	Fjord under ice	—	—	—	0.003–0.113

values of density ratio ($2.5 \leq R_\rho \leq 5$); salt fingers could perhaps explain the ''leveling off'' of this trend at smaller R_ρ values, but our Monte Carlo experiments suggest that measurement error is the most likely explanation.

Acknowledgments. This work is part of the Canadian contribution to WOCE, the World Ocean Circulation Experiment. It was supported by NSERC and Department of Fisheries and Oceans. We thank our colleagues Kurt Polzin, Dan Kelley, Hartmut Peters, and particularly Eric Kunze, for their generous help with the manuscript, and Jim Burke for his help in collecting and analyzing these observations. Maureen Cribb is thanked for helping with the data reduction and analysis.

APPENDIX

The Lognormal Distribution

A lognormal distribution can be used to describe a dataset that is skewed toward large values (i.e., more than half of the points are smaller than the mean, but the larger values tend to be more extreme). The arithmetic mean of a finite number of observations taken from a lognormal distribution is largely dependent on a small number of extremely large values. The arithmetic mean is hence an inefficient estimator of the mean of a lognormally distributed random variable (Baker and Gibson 1987).

A *non-negative* random variable X is said to have a lognormal distribution if its logarithm, the random variable $Y = \ln(X)$, has a normal distribution with expected value μ and variance σ^2. The probability density function (pdf) of X is

$$P(X) = \frac{1}{\sqrt{2\pi}\,\sigma X}\exp\left[\frac{-(\ln(X) - \mu)^2}{2\sigma^2}\right]. \quad \text{(A1)}$$

The expected value of the ith moment can be shown to be

$$E(X^i) = \exp\left[i\mu + \frac{i^2\sigma^2}{2}\right]. \quad \text{(A2)}$$

The mean, median, and mode are not equal as they are for a symmetric distribution like the Gaussian. Using (A2) the mean, or the first moment, is

$$E(X) = \exp\left[\mu + \frac{\sigma^2}{2}\right], \quad \text{(A3)}$$

while the mode, corresponding to the peak in the pdf, is

$$\text{mode}(X) = \exp[\mu - \sigma^2]. \quad \text{(A4)}$$

The median, or 50th percentile, is

$$\text{median}(X) = \exp[\mu]. \quad \text{(A5)}$$

Note that $\text{mean}(X) > \text{median}(X) > \text{mode}(X)$, and the difference increases with the so-called intermittency factor σ^2.

Given a finite number n of samples X_i from a lognormal distribution, Baker and Gibson (1987) show that the arithmetic mean of these samples,

$$\langle X\rangle_{am} = \frac{1}{n}\sum_{i=1}^{n} X_i, \quad \text{(A6)}$$

is an inefficient estimator of the expected value, especially for large intermittency factor. They suggest using the maximum likelihood estimator (MLE)

$$\langle X\rangle_{mle} = \exp\left[m + \frac{s^2}{2}\right], \quad \text{(A7)}$$

where m and s^2 are the arithmetic sample mean and variance of $\ln(X_i)$, computed as

$$m = \frac{1}{n}\sum_{i=1}^{n} \ln(X_i) \tag{A8}$$

and

$$s^2 = \frac{1}{n-1}\sum_{i=1}^{n} [\ln(X_i) - m]^2. \tag{A9}$$

In practice, the observed distributions of ε and χ deviate from lognormality at the low and high ends of the distribution, possibly due to instrumental considerations, but computation of m and s^2 using (26) and (27) is fairly insensitive to these deviations.

a. Confidence intervals for the mean of a lognormal variate

The confidence limits for the mean of $Y_i = \ln(X_i)$ (with a normal distribution) are $\pm z_{\alpha/2}(\sigma/\sqrt{n})$, where the quantity $z_{\alpha/2}$, the $(1 - \alpha)$ confidence coefficient, is defined below. The antilog of this is the confidence interval for the median of X_i; the appropriate confidence interval for the mean of a lognormally distributed variable is (Baker and Gibson 1987)

$$\langle X\rangle_{mle} e^{-z_{\alpha/2}\eta} < E(X) < \langle X\rangle_{mle} e^{+z_{\alpha/2}\eta} \tag{A10}$$

and

$$\eta = \left[\frac{\sigma^2}{n} + \frac{\sigma^4}{2(n-1)}\right]^{1/2}. \tag{A11}$$

In practice, the sample variance s^2 is used for the intermittency factor in 29. To compute 95% confidence limits we take the confidence coefficient in 28 as $z_{\alpha/2} = 1.96$. For 99% confidence limits, we take $z_{\alpha/2} = 2.575$.

To estimate the number of degrees of freedom of the data [denoted by n in (A8)], autocorrelation functions were computed for $\log\Gamma_d$, and correlations were found to be smaller than 0.16 for lags of one segment length ($\sim$8 m) or larger. Hence adjacent data blocks are very nearly statistically independent, so n is equal to the number of observations in a given bin.

REFERENCES

Baker, M. A., and C. H. Gibson, 1987: Sampling turbulence in the stratified ocean: Statistical consequences of strong intermittency. *J. Phys. Oceanogr.,* **17,** 1817–1836.

Clark, D. G., 1997: Physical and biological sources and sinks of nitrate in the Canary Basin. M. Sc. thesis, Dalhousie University, 90 pp.

Davis, R. E., 1996: Sampling turbulent dissipation. *J. Phys. Oceanogr.,* **26,** 341–358.

Farmer, D. M., 1975: Penetrative convection in the absence of shear. *Quart. J. Roy. Meteor. Soc.,* **101** (430), 869–891.

Fleury, M., and R. G. Lueck, 1994: Direct heat flux estimates using a towed body. *J. Phys. Oceanogr.,* **24,** 801–818.

Gargett, A. E., 1988a: Reynolds number effects on turbulence in the presence of stable stratification. *Small Scale Turbulence and Mixing in the Ocean,* J. C. J. Nihoul and B. M. Jamart, Eds., Elsevier Oceanogr. Ser., 517–528.

——, 1988b: The scaling of turbulence in the presence of stable stratification. *J. Geophys. Res.,* **93,** 5021–5036.

——, and J. N. Moum, 1995: Mixing efficiencies in turbulent tidal fronts: Results from direct and indirect measurements of density flux. *J. Phys. Oceanogr.,* **25,** 2583–2608.

Gregg, M. C., 1987: Diapycnal mixing in the thermocline: A review. *J. Geophys. Res.,* **92,** 5249–5286.

Hamilton, J. M., M. R. Lewis, and B. R. Ruddick, 1989: Vertical fluxes of nitrate associated with salt fingers in the world's oceans. *J. Geophys. Res.,* **94,** 2137–2145.

——, N. S. Oakey, and D. E. Kelley, 1993: Salt finger signatures in microstructure measurements. *J. Geophys. Res.,* **98,** 2453–2460.

Howard, L. N., and G. Veronis, 1987: The salt-finger zone. *J. Fluid Mech.,* **183,** 1–23.

Ledwell, J. R., and A. J. Watson, 1994: North Atlantic Tracer Release Experiment—Newest results. WOCE Notes, Vol. 6 (1), 1–4. U.S. WOCE Office, Dept. of Oceanography, Texas A&M University, College Station, TX 77843–3146.

——, ——, and C. S. Law, 1993: Evidence for slow mixing across the pycnocline from an open-ocean tracer-release experiment. *Nature,* **364,** 701–703.

Linden, P. F., 1979: Mixing in stratified fluids. *Geophys. Astrophys. Fluid Dyn.,* **13,** 3–23.

McDougall, T. J., and B. R. Ruddick, 1992: The use of ocean microstructure to quantify both turbulent mixing and salt fingering. *Deep-Sea Res.,* **39** (11/12), 1931–1952.

Moum, J. N., 1996: Efficiency of mixing in the main thermocline. *J. Geophys. Res.,* **101,** 12 057–12 069.

——, D. R. Caldwell, and C. A. Paulsen, 1989: Mixing in the equatorial surface layer and thermocline. *J. Geophys. Res.,* **94,** 2005–2021.

Oakey, N. S., 1982: Determination of the rate of dissipation of turbulent energy from simultaneous temperature and velocity shear microstrucure measurements. *J. Phys. Oceanogr.,* **12,** 256–271.

——, 1985: Statistics of mixing parameters in the upper ocean during JASIN Phase 2. *J. Phys. Oceanogr.,* **15,** 1662–1675.

——, 1988: Epsonde: An instrument to measure turbulence in the deep ocean. *IEEE J. Oceanic Eng.,* **13,** 124–128.

Osborn, T. R., 1980: Estimates of the local rate of vertical diffusion from dissipation measurements. *J. Phys. Oceanogr.,* **10,** 83–89.

——, and C. S. Cox, 1972: Oceanic fine structure. *Geophys. Fluid Dyn.,* **3,** 321–345.

Peters, H., M. C. Gregg, and T. B. Sanford, 1995: Detail and scaling of turbulent over-turns in the Pacific Equatorial Undercurrent. *J. Geophys. Res.,* **100,** 18 349–18 368.

Schmitt, R. W., 1979: Flux measurements on salt fingers at an interface. *J. Mar. Res.,* **37,** 419–436.

Sherman, J. T., and R. E. Davis, 1995: Observations of temperature microstructure in NATRE. *J. Phys. Oceanogr.,* **25,** 1913–1929.

Toole, J., K. Polzin, and R. Schmitt, 1994: Estimates of diapycnal mixing in the abyssal ocean. *Science,* **264,** 1120–1124.

Turner, J. S., 1968: The influence of molecular viscosity on turbulent entrainment across a density interface. *J. Fluid Mech.,* **33,** 639–656.

——, 1973: *Buoyancy Effects in Fluids.* Cambridge University Press, 368 pp.

Yamazaki, H., and T. R. Osborn, 1993: Direct estimation of heat flux in the seasonal thermocline. *J. Phys. Oceanogr.,* **23,** 503–516.